Stoch Environ Res Risk Assess
DOI 10.1007/s00477-015-1070-0

ORIGINAL PAPER

Identification of sub-trends from hydro-meteorological series

Charles Onyutha[1]

Abstract In hydro-meteorological trend analysis, an alteration in the given variable is detected by considering the long-term series as a whole. Whereas the long-term trend may be absent, the significance of hidden (short-durational) sub-trends in the series may be important for environmental management practices. In this paper, a graphical approach of identifying trend or sub-trends using nonparametric cumulative rank difference (CRD) was proposed. To confirm the significance of the visualized trend, the CRD was translated from the graphical to a statistical metric. To assess its capability, the performance of the CRD method was compared with that of the well-known Mann–Kendall (MK) test. The graphical and statistical CRD techniques were applied to detect trends and sub-trends in the annual rainfall of 10 River Nile riparian countries (RNRCs). The co-occurrence of the trend evolutions in the rainfall with those of the large-scale ocean–atmosphere interactions was analyzed. The power of the CRD method was shown to closely agree with that of the MK test under the various circumstances of sample sizes, variations, linear trend slopes, and serial correlations. At the level of significance $\alpha = 5$ %, the long-term trends were found present in 30 % of the RNRCs. However at $\alpha = 5$ %, the main downward (upward) sub-trends were found significant in 30 (60 %) of the RNRCs. Generally at $\alpha = 1$ %, linkages of the trend evolutions in the rainfall of the RNRCs were found to those of the influences from the Atlantic and Indian Oceans. At $\alpha = 5$ %, influences from the Pacific Ocean on the rainfall trends of some countries were also evident.

Keywords Trend analysis · Trend evolution · Sub-trend identification · Nonparametric cumulative rank deviation (CRD) method · Hydro-meteorology · River Nile riparian countries

1 Introduction

Albeit other pressing challenges such as over population, poverty, transboundary water resources management problems and so on in different parts of the world, the issue of global warming due to the increase in greenhouse is undeniably becoming the cynosure of the international endeavour. A high-jacked portion of the said attention is seen in an overwhelming concern sparked off to investigate whether or not there are changes in the hydro-meteorological variables. For only the years 2013–2014, examples of studies related to the said changes include Lavender and Abbs (2013), Nyeko-Ogiramoi et al. (2013), Paruolo et al. (2014), Şen (2014), Tao et al. (2014). The common practice of trend analysis in hydro-meteorology is to consider a long-term series as a whole. Also crucial to consider is the possibility of severe events occurring in the form of clusters over certain periods of the data record length. The occurrence of such clusters above or below the long-term average of the hydro-meteorological variable affects the overall trend by shifting it up or downwards, respectively. Eventually, the trend obtained considering the full time series is typical of the net effect of such shifts. Although the overall trend in a given data may be insignificant, if analyses are separately done over short periods, the sub-trends may be significant. Moreover, the sub-period for the

✉ Charles Onyutha
conyutha@gmail.com

[1] Faculty of Technoscience, Muni University, P.O. Box 725, Arua, Uganda

Published online: 23 April 2015

possible significant sub-trend might be of length quite important to consider for environmental management practices. The identification of the sub-trends and assessment of their significance altogether make it possible to ascertain the likelihood of any intervention on the hydro-meteorological variable by, say, the short-durational climate fluctuations. Such influences can exist in various forms; for instance they may bring about inconsistencies in rainfall data including, among others, observational errors in monitoring and change of recording methodology and equipment (Kampata et al. 2008). Statistical inferences of the insights into the possible interventions on the hydro-meteorology can be useful for practitioners to make appropriate decisions on environmental planning and management. Separating the sub-trends over short-durations (e.g. of decadal time scales) from that of the long-term period (for instance due to global warming) also makes it possible to determine the possible drivers of change in the hydro-meteorological variable under consideration. Analysis of the co-occurrences of the trend evolutions in, say, rainfall and those of the associated possible driving forces which might be from e.g. the large scale ocean–atmosphere interactions can be valuable especially in predicting the upcoming periods of decrease or increase in the variable.

To detect trends, nonparametric tests are more often used than the parametric ones due to their suitability for non-normally distributed data in hydro-meteorology. However, the commonly used methods provide rather statistical than visual exploratory aspects of the trend detection. According to Kundzewicz and Robson (2000), without a proper exploratory data analysis as a very powerful graphical technique, trend test results can be meaningless in some cases. Graphical exploration of changes in a dataset can make it possible to identify significant hidden (short-durational) sub-trends in a series. It can also reveal fascinating facts about the data as well as maximizing understanding which in turn can invite further investigations.

Thus, this paper is aimed at: (1) introducing a graphical approach of identifying linear sub-trends and/or trend, (2) determining the validity of the introduced method, (3) applying the method to analyze trends/sub-trends in the rainfall of the River Nile riparian countries (RNRCs) in Africa, and (4) attempting to explain the drivers of the trends.

2 Trend detection methods

Although the reviews and details of the different trend detection methods can be found in Khaliq et al. (2009), and Sonali and Kumar (2013), the statistical and graphical approaches are briefly mentioned.

2.1 Statistical approaches

Some of the nonparametric trend detection methods include the Mann–Kendall (MK) (Mann 1945; Kendall 1975) and the Spearman's rho tests. The slope m, of a monotonic trend can be given by the method of Theil (1950) and Sen (1968). Because the ability to detect trend is influenced by the autocorrelation in the data, Yue et al. (2002a) proposed a trend-free prewhitening (TFPW) for the case when both trend and lag-1 autoregressive process AR(1) exist in a time series.

2.2 Graphical techniques

To observe changes over time of any trend, the sequential MK test (Modarres and Sarhadi 2009; Sneyers 1990) can be used. In this method, each sample point is considered sequentially in both the progressive and retrograde analyses. On top of the mentioned consideration, in this study, a method of also using moving window of fixed block length (instead of only considering the sample points singly) is proposed to understand the evolution of sub-trends. This is important especially when the cycle length for the oscillatory increase or decrease in the hydro-meteorological variable is known.

Recently, Şen (2012) introduced an innovative trend detection technique in which the first half of the time series is plotted against the second one. If there is no trend in the series, the data points fall on the 1:1 (45°) line. Because the data points are used directly, the presence of possible outliers may affect the trend result from this method. Since the data points in each half of the time series are sorted before plotting, the sequential order of the time period of a possible sub-trend (which may be of the durational length less or greater than half the data record period) cannot also be directly judged from the plot on the Cartesian coordinates. In this study, the methodology proposed considers: (1) ranks of data to reduce the influence of possible outliers, (2) the time series as a whole such that the sub-trend periods are exhibited without the loss of the sequential order of the time periods of data points.

3 Sub-trend identification

3.1 Cumulative rank difference

In assessment of homogeneity, trend or variability in hydro-meteorological series, rescaling of the data is important. One way to do this is through parametric rescaling of the time series as seen from e.g. Buishand (1982) (to analyze homogeneity), Kundzewicz and Robson (2000) (for the cumulative deviation test), Kampata et al. (2008)

(for the distribution free cumulative summation (CUSUM) procedure). The above parametric rescaling entails division of adjusted partial sums by the standard deviation (S_D). This is closely related to the Hurst rescaling (Hurst 1951) where the deviation of each sample point from the mean is accumulated to form an adjusted range which is divided by the S_D. The rescaled range (ratio of the adjusted range to the S_D) is expected to increase asymptotically with the square root of the sample size n. In hydrology, the exponent (also called the Hurst exponent) often deviates from the expected value of 0.5 thereby bringing about the effect termed as the Hurst phenomenon. Interpretations of the Hurst phenomenon tend to be given in terms of persistence, non-stationarity, shift in the record mean etc. In this paper, a method herein referred to as the cumulative rank difference (CRD) is proposed such that concept related the Hurst rescaling is used analogously to rescale time series in a nonparametric way in terms of the difference (D) between the exceedance and non-exceedance counts of data points. The difference is accumulated to obtain the cumulative sum (S_m) which is used to separate sub-trends over unknown periods of increase or decrease in the given variable. The rescaled series is obtained using Eq. (1).

$$D(i) = R_a(i) - R_b(i) = 2R_a(i) - (n - w_i) \quad \text{for } 1 \le i \le n \tag{1}$$

where R_a is the number of times a data point is exceeded, R_b the number of times a data point exceeds others, w_i the number of times a data point appears within the given sample.

The accumulated difference in the ranks is obtained using Eq. (2).

$$S_m(i) = \sum_{j=1}^{j=i} D(j) \qquad \text{for } 1 \le i \le (n) \tag{2}$$

because $\sum\{D(j)\} = 0$, it can be checked that $S_m(n) = 0$.

3.1.1 Graphical CRD approach

Graphically, to identify sub-trends, the S_m (Eq. 2) is plotted against i or the time unit of the series such that

(i) The $S_m = 0$ line represents the reference i.e. an ideal case with completely no trend in the data. The data points below and above the reference is expected to characterize the trend/sub-trends.

(ii) The data points for a monotonically decreasing (increasing) trend take the form of a curve, most part of which, if not entirely, will fall below (above) the reference (see case (c) and (3), (e) and (5), respectively of Fig. 10). The absolute maximum value of S_m (S_{ABS}) in such a case will be clearly far from the reference. For the possible maximum increasing (decreasing) monotonic trend, the curve is expected to take the form of a quadratic function ($Pi^2 + Qi + R$) with constant $P = -1(1)$ and $Q = 1(-1)$. For a large n, the constant R is approximately equal to zero. Thus for a monotonically decreasing or increasing trend, the curve is described by $S_m(i) = \{i^2 - ni\}$ or $S_m(i) = \{ni - i^2\}$, respectively. It is also possible that for the same (given) data, there can be a number of distinctive curves above or below the reference. In such cases, each complete curve above (below) the reference can be taken as a separate upward (downward) sub-trend.

(iii) If a time series has an increasing sub-trend in its first half and a decreasing one in the second, there will be two curves. The first (second) curve will be above (below) the reference; the two curves can be described by a polynomial which crosses the $S_m = 0$ line at $i = 0.5n$ (see case (a) and (1) of Fig. 10).

(iv) When there is no trend in the data, the CRD pattern fluctuate while crossing the $S_m = 0$ line a number of times (see case (b) and (2) of Fig. 10). In such series, the S_{ABS} is small in magnitude, and periods for the sub-trends can vary so much in length.

(v) In the case of step upward jump in the series (assuming no linear trend in the part of the series before and after the jump), the data points take the form of two lines with their vertex above the reference; the first (second) line will have positive (negative) slope (see case (d) and (4) of Fig. 10). However, if there is a step downward jump in the series, the two lines and their vertex will be below the $S_m = 0$ line with the first (second) part having negative (positive) slope.

(vi) If a dataset has two linearly positive sub-trends separated by a downward step jump, the data points will form two curves above the reference (see case (f) and (6) of Fig. 10). For negative sub-trends the curves will be below the reference.

3.1.2 Statistical CRD test

In some cases the significance of the sub-trends identified graphically may be subjective. Eventually, support is required from the statistical CRD test for the conclusiveness of the trend or sub-trend significance. This requires the statistical CRD trend statistic which is derived next in a simplified way.

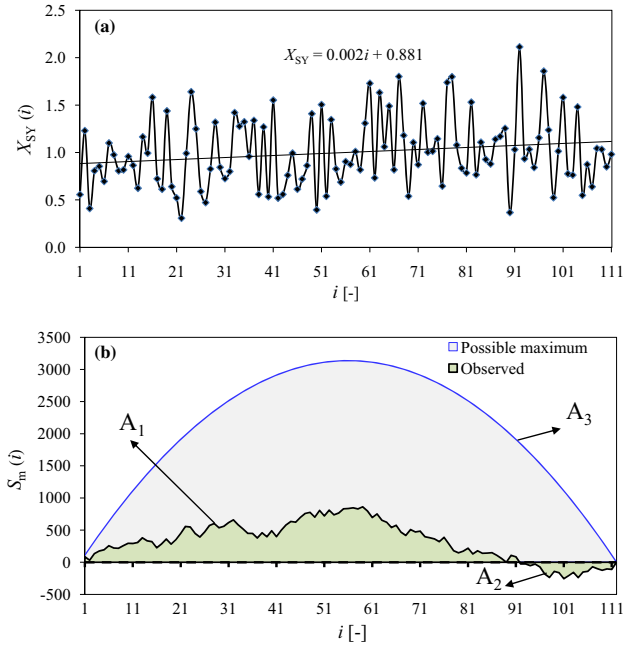

Fig. 1 Graphical visualization of **a** X_{SY} series, **b** CRD results for the X_{SY} series and a possible maximum trend in a dataset of $n = 111$

Consider the plot of $S_m(i)$ versus i in Fig. 1 obtained using a synthetic series X_{SY} of $n = 111$, and let A_1 (A_2) occupying the period from $i = 1$ to 91 (92 to 111) denote the area enclosed by the data points falling above (below) the $S_m(i) = 0$ line, and A_3 the area under curve for the corresponding possible maximum monotonic trend in a dataset of size equal to that of the X_{SY}. It can be noted that A_1 (A_2) indicates positive (negative) sub-trend. Since $|A_1| > |A_2|$, m is positive; otherwise it would be negative. The S_{ABS} is 862 and occurs at $i = 59$.

Statistically, the trend in the given series can be estimated using the net area taken by the data points. From Fig. 1b, the net area which is given by $(A_1 - A_2)$ directly depends on the S_{ABS}. The pattern of the data points may be irregular due to randomness in the series. However, for the possible maximum monotonic trend, the pattern is regular. The net areas for the irregular ($A_{tot,1}$) and regular ($A_{tot,2}$) patterns of data points can be obtained by approximation such that:

$$A_{tot,1} = \sum_{i=1}^{n-1} S_m(i) \tag{3}$$

$$A_{tot,2} = \sum_{i=1}^{n} \left(ni - i^2\right) = n\sum_{i=1}^{n} i - \sum_{i=1}^{n} i^2 \tag{4}$$

According to Hall and Knight (1891) following Carl Friedrich Gauss, $\sum i = n(n+1)/2$ and using the concept of telescoping or collapsing sum, $\sum i^2 = n(n+1)(2n+1)/6$. Making substitutions into Eq. (4),

$$A_{tot,2} = \frac{n^2(n+1)}{2} - \frac{n(n+1)(2n+1)}{6} = \frac{(n^3 - n)}{6} \tag{5}$$

To scale and/or standardize the order of magnitude of the net area, $A_{tot,1}$ can be divided by $A_{tot,2}$ and eventually the CRD trend statistic (T_{CRD}) is obtained as in Eq. (6).

$$T_{CRD} = \frac{6}{(n^3 - n)} \sum_{i=1}^{n-1} S_m(i) \tag{6}$$

A monotonically increasing (decreasing) trend in the data is shown by $T_{CRD} > 0$ ($T_{CRD} < 0$). The maximum (minimum) possible value of T_{CRD} is 1(−1).

3.1.3 *Testing the significance of the trend from the statistical CRD test*

To test the significance of the trend using the computed T_{CRD} (Eq. 6), the null hypothesis (H_0) that "there is no trend in the series" can be considered. Without any commitment to the possible non-trivial mathematics/statistics, the H_0 can be verified at a given level of significance α % by constructing the hypothesis rejection/acceptance boundary in the form of $(100 - \alpha)$ % confidence interval (CI) using nonparametric Monte Carlo bootstrapping (Davidson and Hinkley 1997). The trend is significant if the computed T_{CRD} up or down-crosses the constructed $(100 - \alpha)$ % CI. To reduce the computational demand of the bootstrapping procedure, critical values for verifying the H_0 is derived next. This is however, for brevity only carried out for series with untied ranks of data points. Consider N_{MC} (the number of Monte Carlo simulations) set to a value of 1000 due to the computational load; the thresholds for verifying the H_0 were generated using the flow chart below:

(1) Set $\alpha = 10$, 5 or 1 %;
(2) Make $n = 10(10)110$;
(3) For the selected n, generate N_{MC} synthetic series;
(4) For each series, perform TFPW where necessary and compute T_{CRD} using Eq. (6); this will yield N_{MC} values of T_{CRD};
(5) Rank the values of the computed T_{CRD} from the highest to the lowest;
(6) Pick the $[0.005 \times \alpha\ \% \times N_{MC}]$th value of the T_{CRD};
(7) Repeat steps (3) to (6) till 100 values are obtained from step (6);
(8) Calculate and take the average of the 100 T_{CRD} values of step (7) as the threshold to accept/reject H_0;
(9) Go to the next n and repeat steps (2) to (8), and
(10) Go to the next α % and repeat steps (1) to (9).

Due to the randomness in the values of the T_{CRD} resulting from the above flow chart, the need to fit a theoretical distribution that can best describe the variation of the threshold with n was inevitable. To do this, Eq. (7) was used since the decrease of the threshold with n was expected to follow a power function.

$$f(n) = \frac{a}{n^b} \tag{7}$$

where $f(n)$ represents the critical value of the T_{CRD}; a and b are constants.

Consider $T_{e,i}$ as the values of the T_{CRD} obtained from the flow chart above, $T_{g,i}$ the theoretical critical values computed using Eq. (7), and $T_{r,i}$ the residual in terms of the difference between $T_{e,i}$ and $T_{g,i}$; to determine the constants a and b of Eq. (7), power trendlines were fitted to the plot of $T_{e,i}$ versus n and the corresponding equations are shown in Fig. 2a. The 'goodness-of-fit' between the $T_{e,i}$ and $T_{g,i}$ (Fig. 2a) were assessed both graphically and statistically.

Graphically, the values of the residuals $T_{r,i}$ were plotted against: (1) the standard normal variate (z) i.e. normal probability plot (Fig. 2b), (2) their relative frequency (Fig. 2c), and (3) cumulative probability distribution (Fig. 2d). It can be noted that plots in Fig. 2b, c and d show a straight line, bell-shape and sigmoid curve, respectively. These altogether show that the residuals follow the Gaussian distribution as expected. It can be seen from Fig. 2a that, as n gets larger, the threshold becomes smaller. This is because the statistical uncertainty due to the limitation of sample points is higher when n is smaller. It is also known that a trend test becomes more powerful with higher than lower values of n (Yue et al. 2002b). It can be noted that the optimal value of b of Eq. (7) is 0.5. This has a physical meaning i.e. it is because a sum is considered, that is why the variation of the T_{CRD} with n has a connection with the square root of n.

Statistically, the Kolmogorov–Smirnov (K–S) (Kolmogorov 1933; Smirnov 1936) test (Eq. 8) at $\alpha = 5$ % was conducted on the H_0 that the variation of the threshold with n followed a power function. Comparison was made between the K–S statistic (K_{stat}) and the critical values (K_{CV}) of the said test. The H_0 was accepted if K_{stat} was found to be less than K_{CV}; otherwise it was rejected. The K_{stat} was computed as:

$$K_{stat} = \underset{i=1}{\overset{n}{Max}}\left\{F\left(T_{e,i}\right) - F\left(T_{g,i}\right)\right\} \tag{8}$$

where $F(T_{g,i})$ and $F(T_{e,i})$ are the cumulative distributions of $T_{g,i}$ and $T_{e,i}$, respectively.

The K–S was supported by the Anderson–Darling (Anderson and Darling 1952) test (Eq. 9-10), the root mean squared error RMSE [–] (Eq. 11), the *bias* [%] (Eq. 12), and the probability plot correlation coefficient PPCC [–] (Vogel 1986) (Eq. 13). The Anderson–Darling statistic (AD) was computed after sorting the values of $T_{r,i}$ in ascending order. The H_0 that the values of $T_{r,i}$ followed a Gaussian distribution was used.

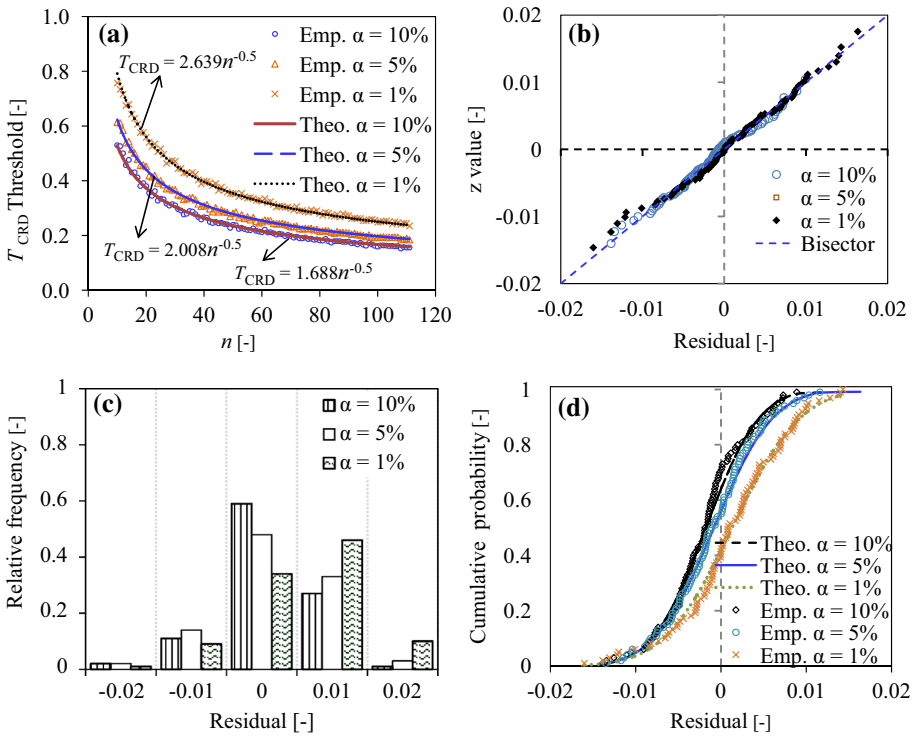

Fig. 2 **a** Variation of hypothesis testing threshold with n, **b** normal probability plot of residuals, **c** relative frequency distribution of residuals, **d** cumulative probability distribution of residuals. In the legends, 'Theo.' and 'Emp.' stand for theoretical and empirical distributions, respectively

$$AD = -n - \frac{1}{n}\sum_{i=1}^{n}(2i-1)\left[\ln F\left(T_{r,i}\right) + \ln\left(1 - F\left(T_{r,(n-i+1)}\right)\right)\right] \quad (9)$$

where $F\ (T_{r,i})$ is the cumulative distribution of $T_{r,i}$. To account for the effect of a small n, an adjusted AD (AD*) Eq. (10) was required to compute the p value following Stephens (1986).

$$AD^* = AD\left(1 + \frac{3}{4n} + \frac{9}{4n^2}\right) \quad (10)$$

At $\alpha = 5$ %, if the p value for the AD* was greater than 0.05, the H_0 was accepted; otherwise rejected.

$$RMSE\,[-] = \left(\frac{1}{n}\sum_{i=1}^{n}\left(T_{e,i} - T_{g,i}\right)^2\right)^{0.5} \quad (11)$$

$$Bias\,[\%] = \frac{1}{n}\sum_{i=1}^{n}\left(\frac{T_{e,i} - T_{g,i}}{T_{g,i}} \times 100\right) \quad (12)$$

$$PPCC\,[-] = \frac{\sum_{i=1}^{n}\left(T_{e,i} - \bar{T}_{e,i}\right)\left(T_{g,i} - \bar{T}_{g,i}\right)}{\left(\sum_{i=1}^{n}\left(T_{e,i} - \bar{T}_{e,i}\right)^2\sum_{i=1}^{n}\left(T_{g,i} - \bar{T}_{g,i}\right)^2\right)^{0.5}} \quad (13)$$

where $\bar{T}_{g,i}$ and $\bar{T}_{e,i}$ are the mean values of $T_{g,i}$ and $T_{e,i}$, respectively.

The statistical 'goodness-of-fits' results are shown in Table 1. It can be noted that the H_0 was accepted in both the K–S and AD tests, the values of RMSE and *bias* [%] were very low, and those of the PPCC were all very close to unity (the best value). These statistics confirm the acceptability of the match between $T_{e,i}$ and $T_{g,i}$ (Fig. 2a). Although $\alpha = 0.5$ % is rarely used in hypothesis testing, its value of a (b) (though not shown in Table 1) was 2.879 (0.5).

To apply the statistical CRD test, if the absolute value of the T_{CRD} computed using Eq. (6) is less than the critical value $f(n)$ from Eq. (7), H_0 (no trend) is accepted; otherwise rejected. Illustratively, for the synthetic X_{SY} series shown in Fig. 1, the absolute $T_{CRD} = 0.192$ which was greater than the $f(n) = 0.191$, indicating a significant upward trend at $\alpha = 5$ %.

Importantly, for the uniformity of the T_{CRD} irrespective of n, an adjusted T_{CRD} (T_{ADJ}) can be computed using Eq. (14). Because the maximum trend in a series has T_{CRD} as one, the adjusted absolute critical value for a given α % becomes approximately equal to one as well. Therefore, it means that trend in the given series is significant if the $T_{ADJ} > 1$; otherwise insignificant. This adjustment of the T_{CRD} is important for assessing trend evolution as will be applied later on.

$$T_{ADJ} = \frac{n^b}{a} \times T_{CRD} \quad (14)$$

where the constants a and b are similar to those of Eq. (7).

3.2 Power of trend tests

Before applying the statistical CRD test, its performance in comparison with that of the MK test was assessed under various circumstances of sample sizes, variations, linear trend slopes, and AR (1). This was, for brevity, done while considering the full time series with untied ranks of data points. The idea was that, if the statistical CRD test could be valid to detect trend in the long-term time series, it would acceptably be applied to statistically support the visualized results of sub-trends from the graphical approach. It is known that two types of errors exist in statistical hypothesis testing. Type I error (also denoted as α %) is the probability of rejecting the H_0 i.e. "there is no trend in the data", when it is true; and type II error is the probability of accepting H_0 while it is false. Eventually, the power of a test is the probability of correctly rejecting the H_0, when it is false. The rejection rates of the trend tests were investigated using large statistical simulations by the Monte Carlo approach based on first-order (Markov) AR stochastic process:

$$X_i = E(X) + r_1(X_{i-1} - E(X)) + \varepsilon_i + L_i \quad (15)$$

where $E(X)$ is the mean of the X_i process, ε_i is the white-noise process with mean $\mu_\varepsilon = 0$ and standard deviation $\sigma_\varepsilon = S_D(1 - r_1^2)^{0.5}$. The linear trend component $L_i = mi$. Following Yue et al. (2002a), for the simulations, X_0 is set to $E(X)$ and $E(X) = 1$; this makes the sample S_D equal the coefficient of variation $C_V(X)$ of X_i. Considering ξ_i as a normally distributed random variable with mean $\mu_\xi = 0$ and standard deviation $\sigma_\xi = 1$, Eq. (15) becomes:

Table 1 Statistics for the match between $T_{g,i}$ and $T_{e,i}$ for variation of threshold with α %

α (%)	a	b	K_{stat} (K_{cv})	AD* (p value)	Bias (%)	RMSE (–)	PPCC (–)
10	1.688	0.5	0.054 (0.135)	0.439 (0.293)	−0.707	0.007	0.9997
5	2.008		0.042 (0.135)	0.162 (0.945)	−0.293	0.006	0.9999
1	2.639		0.051 (0.135)	0.349 (0.473)	0.545	0.008	0.9998

$$X_i = E(X) + r_1(X_{i-1} - E(X)) + C_v(X) \times \xi_i\left(1 - r_1^2\right)^{0.5} + mi \quad (16)$$

The following flow chart was used for comparing the test power:

(i) Set $C_v(X) = 0.25(0.25)0.75$;
(ii) Make $n = 40(20)100$;
(iii) Let $r_1 = 0.0(0.1)0.4$;
(iv) Put $m = -0.0002(0.0001)0.0002$;
(v) Using Eq. (16), generate X_i series characterized by values from steps (i) to (iv);
(vi) Re-compute r_1; if it is significant, perform TFPW on the series from step (v);
(vii) Repeat steps (v) to (vi) till the number of the X_i series obtained reach $N_{MC} = 1000$;
(viii) Test H_0 (no trend) at $\alpha = 5$ % by each method and evaluate its power of test as ratio of the number of rejections of H_0 over N_{MC}, and
(ix) Go to the next value of m, r_1, n, and $C_v(X)$ so as to repeat the above steps accordingly.

The comparative rejection rates for the CRD and MK tests under different variations in the samples are shown for

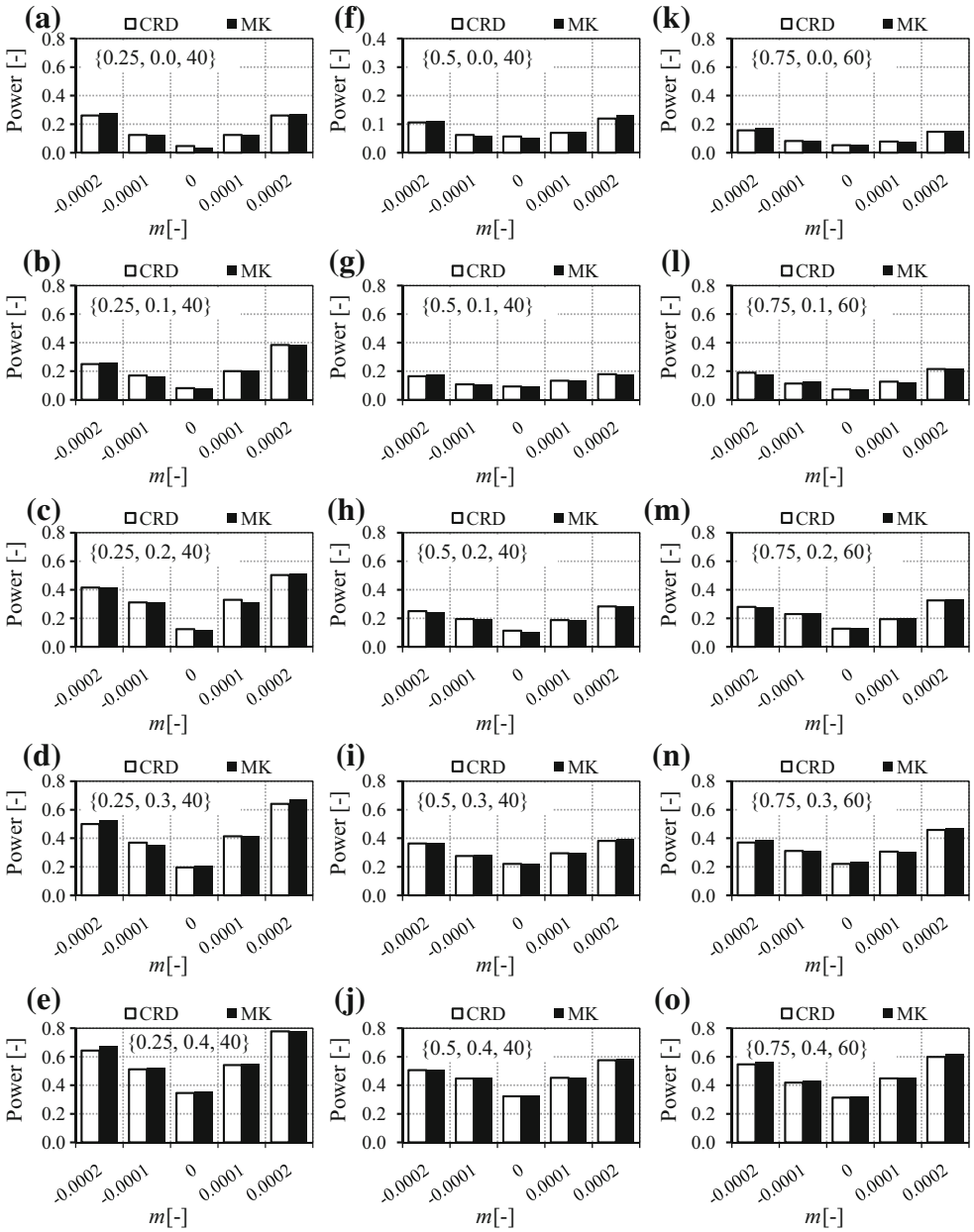

Fig. 3 Comparison of the power of trend test for different values of m; the charts are labeled such that {0.25, 0.1, 40} denote $\{C_v(X) = 0.25, r_1 = 0.1, n = 40\}$

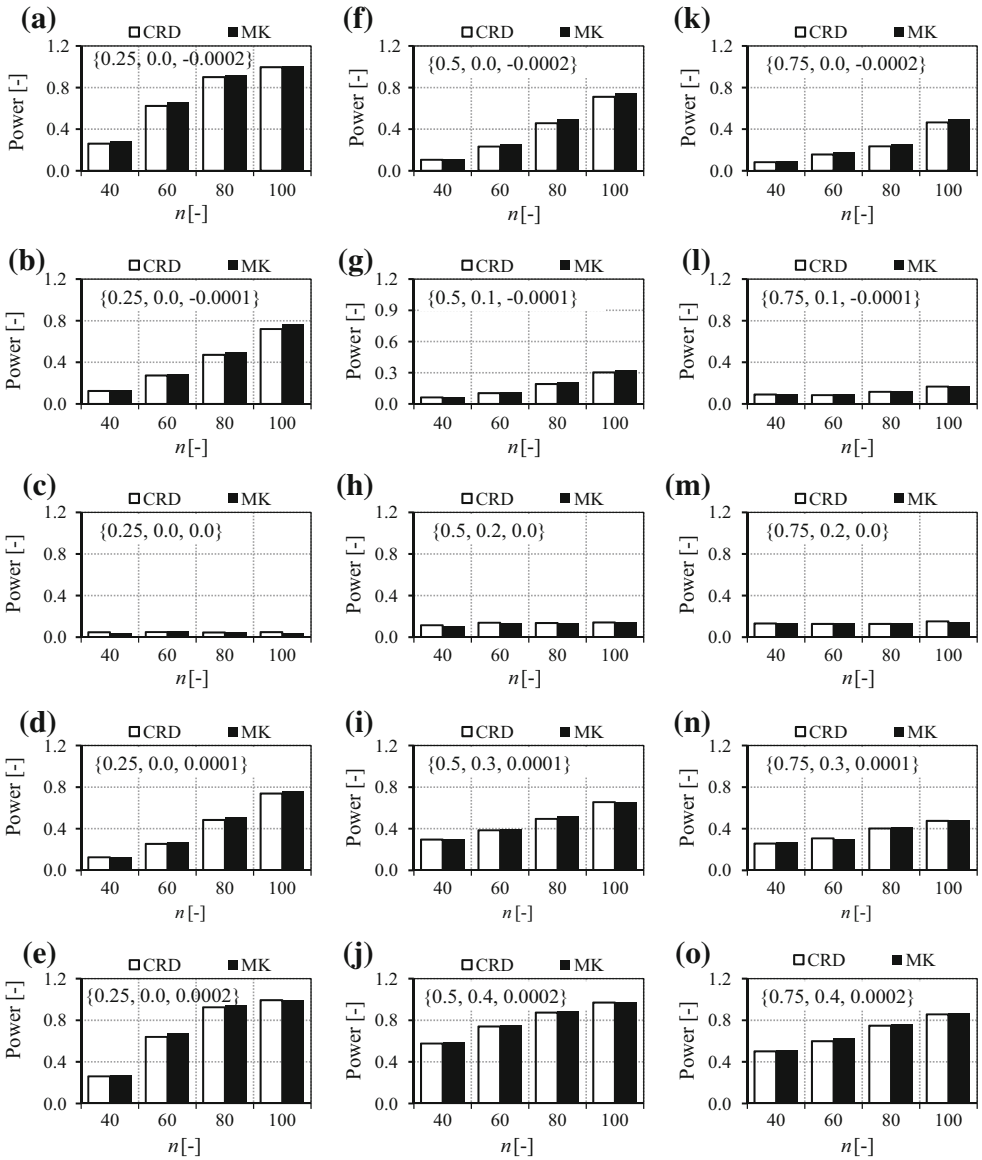

Fig. 4 Comparison of the power of trend test for different values of n; the charts are labeled such that {0.75, 0.3, 0.0001} denote $\{C_v(X) = 0.75, r_1 = 0.3, m = 0.0001\}$

m (Fig. 3), n (Fig. 4) and r_1 (Fig. 5). It is shown in Fig. 3 that as the absolute value of m becomes bigger, the rejection rate increases. It is seen in Fig. 4 that as n increases, the tests become more powerful. The results shown in Figs. 3 and 4 are consistent with those found by Yue et al. (2002b) when comparing the powers of MK and Spearman's rho tests. It can be noted from Fig. 5 that as the value of r_1 increases, the rejection rates increase as well. It is generally shown that when the $C_v(X)$ increases, the tests become less powerful. This, again, is consistent with the finding of Yue et al. (2002b). The details and explanations for the obtained patterns can be taken similar to those from Yue et al. (2002a, b). Importantly, the rejection rates of the CRD and MK were shown to closely agree with each other under the various circumstances of the tests. This confirmed the acceptability of the statistical CRD test to support visualization result from its graphical approach for trend detection and hence, identification of monotonic subtrends.

3.3 Trend evolution

To investigate the evolution of trend in the time series, use can be made of a window or time slice with either fixed and/or varying block length (BL). A BL is the sub-period of the full time series covering the data points of interest.

3.3.1 Moving window of varying block length

A window with varying BL can be applied in both forward (F_{OW}) and backward (B_{CK}) way. In the F_{OW}, the beginning part of the time slice is fixed and its BL constantly

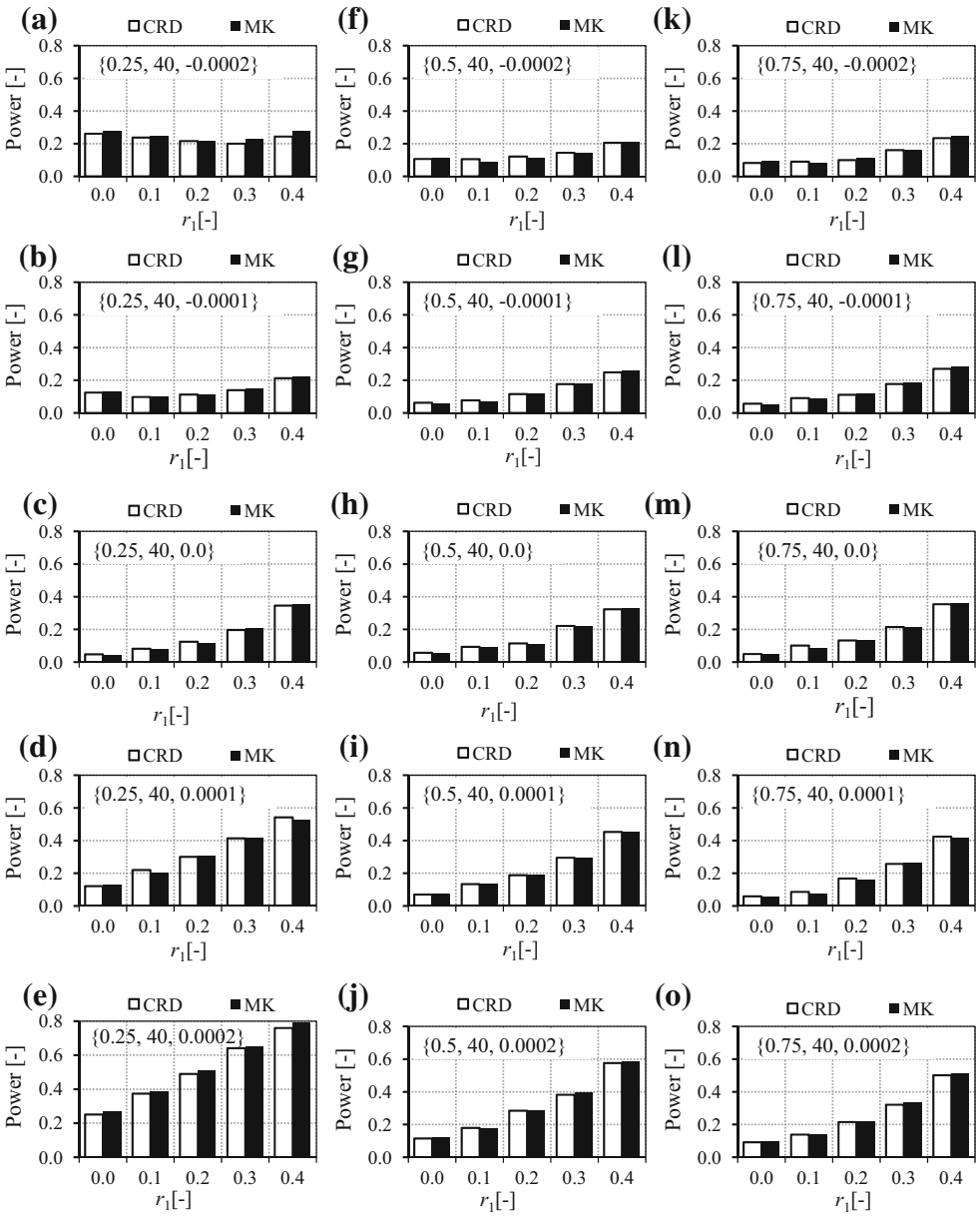

Fig. 5 Comparison of the power of trend test for different values of r_1; the charts are labeled such that {0.5, 40, 0.0002} denote $\{C_v(X) = 0.5, n = 40, m = 0.0002\}$

increased by a unit. Consider the data years 1900, 1901…2000; if the BL of 10 years (as adopted for the statistical CRD test) is moved each time by 1 year, the resulting time slices would cover the periods 1900–1909, 1900–1910… and 1900–2000, respectively. To assess sub-trends using the B_{CK}, the end part of the time slice is fixed on the last point of the time series and its BL constantly increased by a unit. Again, using the same data years as above, the resulting time slices would cover the periods 1991–2000, 1990–2000… and 1900–2000. Over each slice, for the F_{OW} (B_{CK}) method, T_{ADJ} is computed and plotted against the ending (starting) year of the time slices. The lower (LL) and upper (UL) limits of the $(100 - \alpha\ \%)$ CI can be taken as -1 and 1, respectively.

3.3.2 Moving window of fixed block length

On the other hand, a moving window with a fixed BL (F_{BL}) can also be applied. Consider for instance the data years 1901, 1902…2011; if a BL of, say, 20 years is selected and moved each time by 1 year, the resulting time slices would cover the periods 1901–1920, 1902–1921… and 1992–2011, respectively. Over each time slice or sub-period, trend analysis is separately carried out. To obtain a

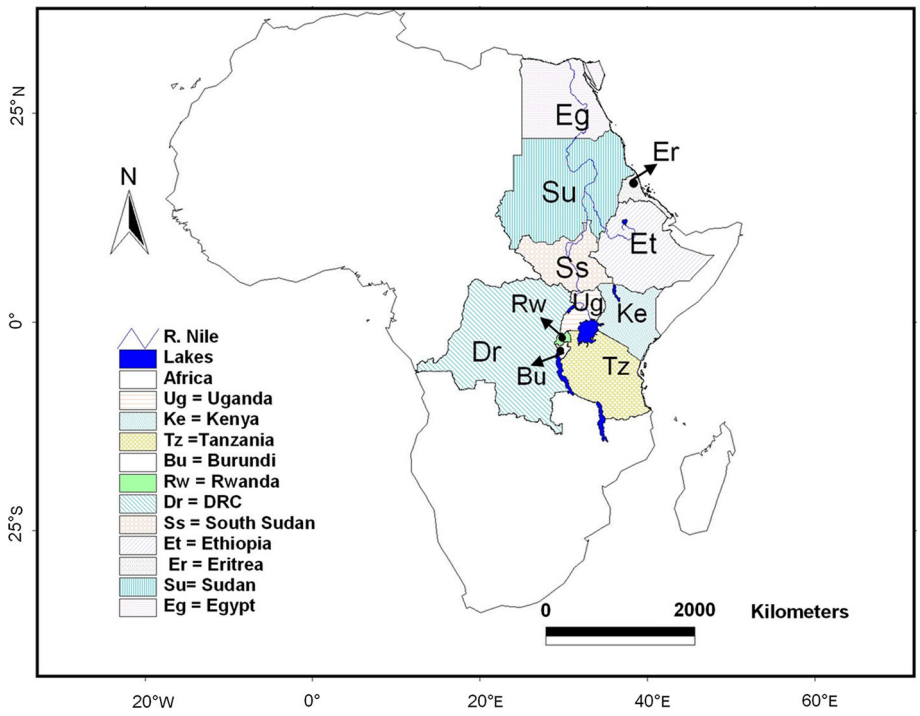

Fig. 6 River Nile riparian countries; *DRC* denotes Democratic Republic of Congo

complete picture of the trend evolution, the values of the T_{ADJ} are plotted against the ending year of the time slices.

4 Case study

4.1 Study area and data

To apply the various techniques of this study including the identification of sub-trends, use of the statistical CRD trend test, and the investigation of trend evolutions, the country-wide long-term monthly rainfall data (Harris et al. 2014) from the British Atmospheric Data Centre (BADC) over the period 1901–2011 for the RNRCs (Fig. 6), and series related to large-scale ocean–atmosphere interactions were used. The monthly climate indices included the southern oscillation index (SOI) based on Ropelewski and Jones (1987), the Atlantic multidecadal oscillation (AMO) index (van Oldenborgh et al. 2009), the Pacific decadal oscillation (PDO) index (Mantua et al. 1997), and the Indian Ocean dipole (IOD). The climate indices were used to gain an insight into the consequence on rainfall trend due the pressure changes occurring in different oceans and the anomaly in circulation due to the sea surface temperature. Since these rainfall data and climate indices were similar to those used by Onyutha (2014), the descriptive details of the study area (Fig. 6), data sources and the quality assurance checks for the time series used in this study can be found from the cited reference. From the monthly series, annual rainfall totals and the mean of the climate indices in each year were obtained for the trend/sub-trend analyses.

4.2 Long-term trend and sub-trends

The long-term trend and sub-trends were identified using the graphical CRD approach. Although it can possible to have several local sub-trends within a given series, for brevity of analysis, two main sub-trends (one positive and the other negative) were considered. The significance of the sub-trends/trend was assessed using the statistical CRD test. The linear trend slope m was computed using the method of Theil (1950) and Sen (1968).

4.3 Drivers of trend

The evolution of trends in the rainfall series and climate indices were assessed using the F_{BL}, F_{OW} and B_{CK} methods. Under the H_0 that 'there is no correlation between the pattern of trend evolution in the rainfall and those of the climate indices', verification of the hypothesis was carried out both at $\alpha = 5$ and 1 %.

4.4 Results

4.4.1 Trends and sub-trends

Figure 7 shows trends and sub-trends in the annual rainfall of the RNRCs. It is shown in Fig. 7d,e that most parts (the

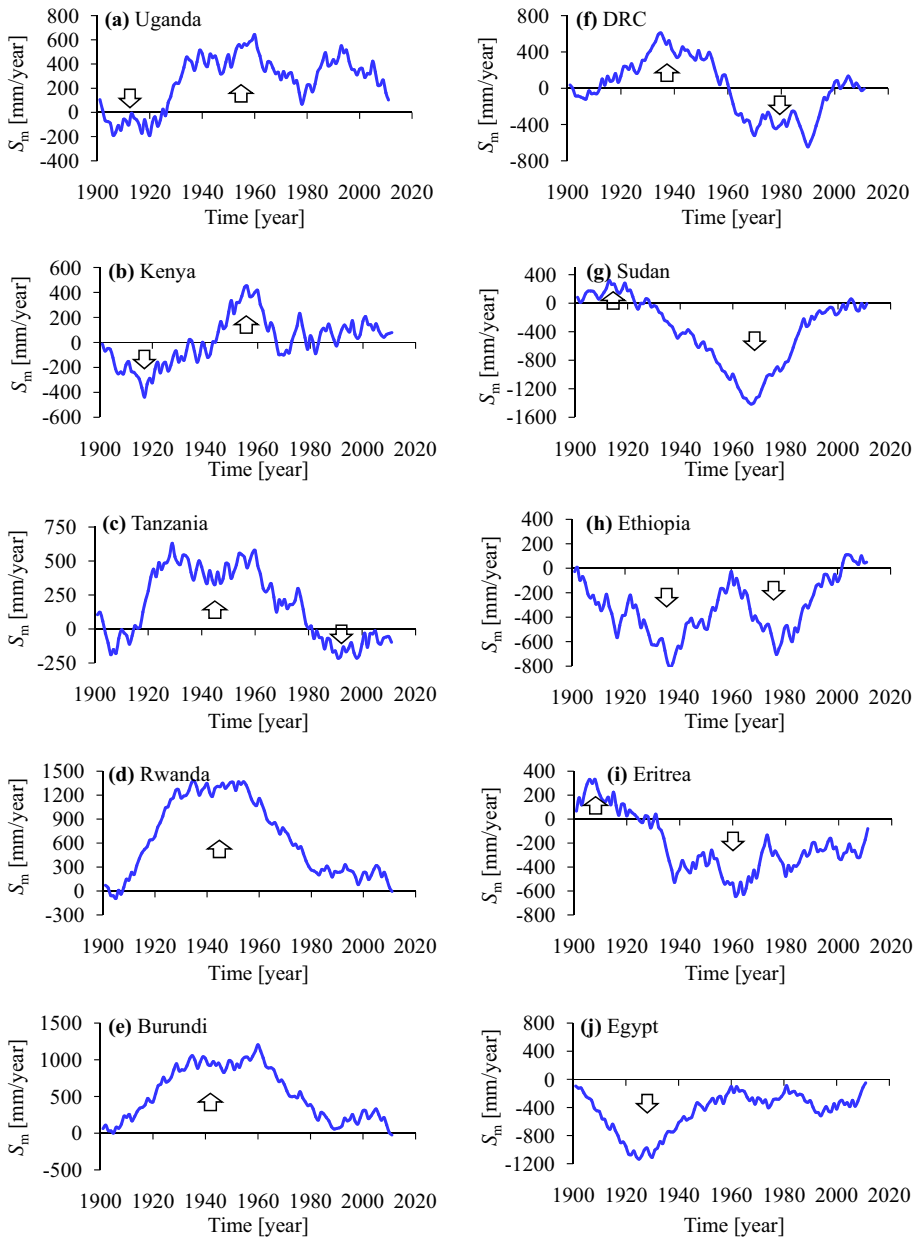

Fig. 7 CRD plots for annual rainfall of the different countries; *up* (*down*) *arrow* shows the main increasing (decreasing) sub-trend

peaks) of the curves formed by the data points clearly fall on one side of (far from) the $S_m = 0$ line. This shows that there was a significant upward trend in annual rainfall in Rwanda and Burundi. In a similar way, from Fig. 7j, it can be noted that there was a significant decreasing trend in the rainfall of Egypt. For the rainfall of Democratic Republic of Congo (DRC) (Fig. 7f), two main sub-trends existed; one was positive and covered the period 1912–1960 and the other from 1961 to 2000 was negative. It is also possible that the sub-trends can be in the same direction. In this same line, for the downward trend in the Ethiopian rainfall from 1902 to 2002, the linear trend slopes m (in mm/year) for the periods before and after the 1960 were different. In some cases, the overall trend in a given series can be dominated by either positive or negative sub-trend; for instance, see the upward (downward) sub-trend in the rainfall of Tanzania (Sudan) in Fig. 7c (g). Considering the full series, in Fig. 7a–f, it is shown that the annual rainfall of the equatorial region was characterized by positive trend though graphically not conclusive for Kenya and DRC. Using station-based observed rainfall, Kizza et al. (2009) and Nyeko-Ogiramoi et al. (2013) also found that trends in rainfall of Lake Victoria basin in the equatorial region of the RNRCs were mainly positive. However, from Sudan up

Table 2 Statistical results of trend analysis

S no.	Country	Full time series			Main downward sub-trend				Main upward sub-trend			
		T_{CRD}	m	r_1	Period	T_{CRD}	m	r_1	Period	T_{CRD}	m	r_1
1	Uganda	0.10	0.57	−0.01	1902–1926	−0.10	−2.36	−0.27	1927–2011	**0.21**	0.97	0.09
2	Kenya	0.01	0.11	0.10	1901–1940	−0.18	−1.50	0.05	1944–1967	**0.46**	9.74	0.02
3	Tanzania	0.11	0.48	0.05	1981–2011	−0.21	−1.42	−0.37	1919–1980	**0.31**	2.12	0.11
4	Rwanda	**0.32**	1.38	0.11	1902–1909	−0.74	−42.39	0.00	1910–2011	**0.34**	1.59	**0.20**
5	Burundi	**0.27**	1.19	0.17	***	***	***	***	1901–2010	**0.27**	1.19	0.16
6	DRC	0.01	0.01	**0.32**	1961–2000	**−0.50**	−3.96	**0.45**	1912–2960	**0.32**	1.55	−0.01
7	Sudan	−0.18	−0.29	**0.27**	1928–2005	**−0.45**	−0.90	**0.36**	1910–1923	0.34	2.54	0.12
8	Ethiopia	−0.17	−0.56	0.15	1902–2002	−0.20	−0.69	0.15	2003–2011	0.28	5.14	−0.31
9	Eritrea	−0.09	−0.23	−0.05	1931–2011	−0.18	−0.75	−0.04	1901–1925	0.28	3.30	−0.12
10	Egypt	**−0.21**	−0.07	−0.02	1901–2011	**−0.21**	−0.07	−0.02	***	***	***	***

*** Nil

Bold values of T_{CRD} and r_1 are significant at level $\alpha = 5$ %

to Egypt (Fig. 7g–j) the annual rainfall trends were all negative. For the conclusiveness of the sub-trend significance, results from the statistical CRD test are compiled in Table 2.

Table 2 shows statistics of rainfall trend and sub-trend results. The bold values of T_{CRD} and r_1 are significant at $\alpha = 5$ %. The CRD critical value at $\alpha = 5$ % for the trend in the full series of each country is 0.187. Considering the full time series, significant upward (downward) trend was found in Rwanda and Burundi (Egypt); this is consistent with results from Fig. 7. The main upward sub-trends in the equatorial region (stations 1–6 from Table 2) were all significant. Downward sub-trends were significant in the rainfall of DRC, Sudan and Egypt. It can be noted that the magnitudes of m in the sub-trends were higher than those in the overall trends of the full series.

Figure 8 shows results of rainfall trend evolution assessed using the various methods. It is shown in the variation of sub-trends with time e.g. for the F_{OW} method that, there was the tendency of the trend in the rainfall over the equatorial region to change from negative to positive while for the countries in the upper half of the Nile Basin i.e. Sudan, Ethiopia, Eritrea and Egypt, it was instead from positive to negative. It means that as the rainfall was decreasing in the southern part of the Nile Basin, in the northern half it was increasing. This difference could suggest that the driving forces for the rainfall trends in these regions are opposite in sign.

4.4.2 Possible drivers of the rainfall trends

Figure 9 shows, for the F_{OW} method, the graphical comparison of the trend evolution patterns in the rainfall of Ethiopia and those of the climate indices. The trend pattern in the rainfall is best followed by that of the AMO, and next by the SOI. This means that the trend in the rainfall over Ethiopia can be partly explained by that in the influences from the Atlantic and Pacific Oceans. For all the RNRCs and the different methods, correlations between rainfall trends and those of climate indices/series as illustrated in Fig. 9 are summarized in Table 3.

In Table 3 the absolute critical value of the correlation coefficients at $\alpha = 5$ % (1 %) using both the F_{OW} and B_{CK} methods is 0.20 (0.26). Correspondingly, using the F_{BL} method, the absolute critical value is 0.21 (0.27) for SOI and 0.20 (0.26) for PDO, AMO and IOD. The difference, among countries, in the magnitudes and sometimes signs of the correlation coefficients could be related to the randomness in the rainfall data or difference in micro-climate (micro-scale features), and the influence of the regional features (topography, water bodies, land cover etc.). Considering the two regions, the equatorial (Uganda, Kenya, Tanzania, Rwanda, Burundi and DRC) and the countries in the northern part of the Nile Basin i.e. Sudan, Ethiopia, Eritrea and Egypt (SEEE), it can be noticed that the driving influences (the correlations) for their rainfall trends seem to be opposite in sign. This, for the F_{OW} method, can be confirmed using correlations between rainfall and IOD or SOI. This, of course, follows from the differences in the trend evolutions as already explained and seen from Fig. 8. The correlations obtained for the F_{BL} method were lower in magnitude than those for the F_{OW} and B_{CK}. This could suggest that the BL of 20 years used, was perhaps, not very representative to describe the periods for the sub-trends. To use the F_{BL} method, it is recommended that a sensitivity analysis be carried out. Although this wasn't done in this

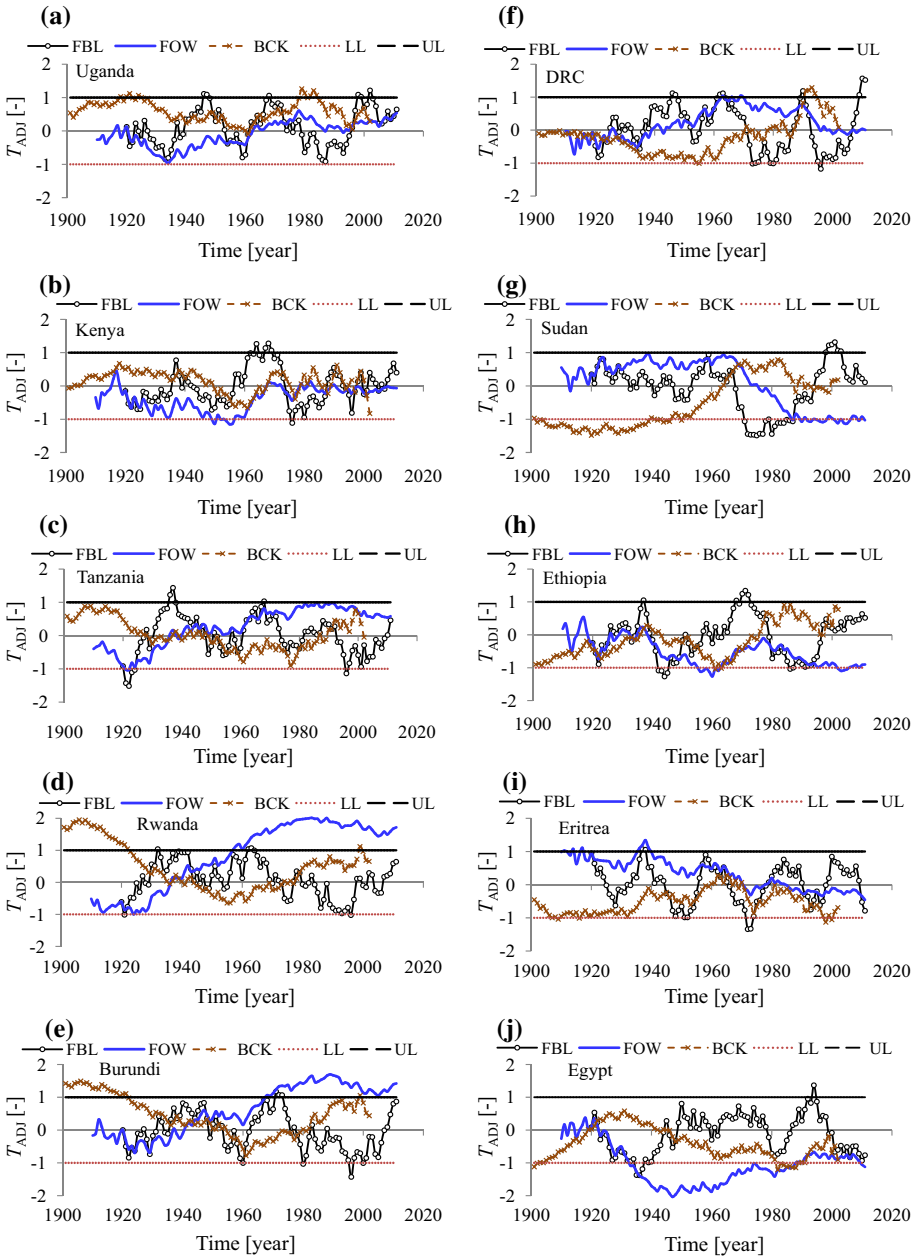

Fig. 8 Trend evolution in the annual rainfall of the different countries obtained using moving window with block length fixed (F_{BL}) or varying in forward (F_{OW}) or backward (B_{CK}) way together with the lower (LL) and upper (UL) limits of the 95 % confidence intervals

study (for brevity), in a trial and error procedure, different values of the BL can be selected and used to determine which trend evolution pattern is representative of the sub-trends in the study area.

It is shown that trends in the rainfall over the equatorial region were significantly caused by those in the influences from the Indian Oceans. A similar result was also found by Camberlin (1997) Tierney et al. (2013) and Onyutha and Willems (2014). Using the F_{OW} method, it can be seen that significant negative (positive) correlations were also found with the SOI (IOD). For the SEEE, significant correlations of the rainfall trends were mainly found with those of the AMO, SOI and IOD. For rainfall variability in Ethiopia, links to the influence from the Pacific and Atlantic Oceans (in terms of SOI and AMO, respectively) have been found by Jury (2010) for the northern and the southern zones, Taye and Willems (2012) and Moges et al. (2014) for the Blue Nile basin.

5 Applying the introduced methodology

The following three main steps are important after applying the TFPW where necessary:

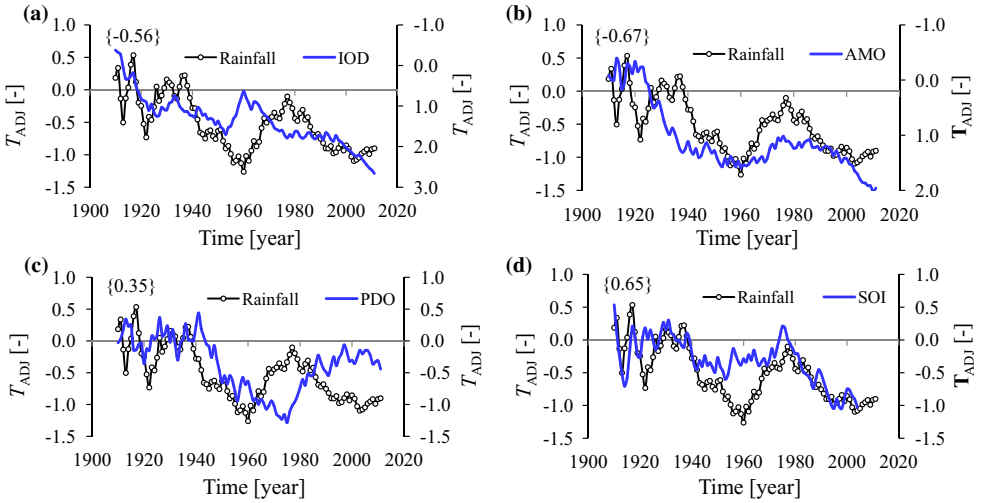

Fig. 9 Trend evolution results for the rainfall and climate indices; the correlation coefficient between the two curves of each chart is put as label in {}

Table 3 Correlation between trend evolution of the rainfall and those of climate indices

B_{CK}					F_{OW}				F_{BL}			
Country	PDO	SOI	IOD	AMO	PDO	SOI	IOD	AMO	PDO	SOI	IOD	AMO
Uganda	**−0.59**	0.17	**0.32**	**0.34**	**−0.53**	**−0.39**	**0.55**	**0.29**	**−0.37**	0.08	**0.53**	−0.06
Kenya	−0.25	−0.07	**0.31**	0.04	−0.13	**−0.26**	0.25	−0.04	0.10	0.01	−0.22	0.15
Tanzania	**−0.29**	**−0.33**	**0.50**	0.21	**−0.54**	**−0.59**	**0.66**	**0.75**	**0.52**	−0.21	**−0.40**	0.18
Rwanda	**−0.62**	−0.12	**0.56**	**0.48**	**−0.67**	**−0.53**	**0.72**	**0.77**	0.00	**0.33**	−0.23	0.19
Burundi	**−0.49**	−0.21	**0.58**	**0.27**	**−0.56**	**−0.59**	**0.71**	**0.61**	0.04	−0.09	0.19	−0.10
DRC	**−0.70**	**0.61**	**−0.37**	−0.01	**−0.83**	−0.15	0.25	**0.50**	0.01	−0.13	−0.23	**0.29**
Sudan	−0.25	**0.73**	**−0.76**	−0.02	−0.01	**0.66**	**−0.68**	**−0.29**	**−0.38**	**0.30**	0.09	**0.58**
Ethiopia	**−0.38**	**0.76**	**−0.56**	**−0.54**	**0.35**	**0.65**	**−0.56**	**−0.67**	−0.17	**0.55**	**0.29**	−0.19
Eritrea	**0.42**	0.24	**−0.44**	−0.02	**0.46**	**0.58**	**−0.82**	**−0.58**	0.25	0.15	**−0.39**	**0.38**
Egypt	**0.29**	**−0.51**	**0.32**	**−0.43**	**0.43**	0.14	**−0.29**	**−0.75**	−0.23	−0.15	−0.02	**−0.50**

Bold values are significant at level $\alpha = 5$ %

(1) Separation of the sub-trends using the graphical CRD approach by:

   (i) Rescaling of the given series using Eq. (1)
   (ii) Calculating cumulative sum (S_m) of the rank difference using Eq. (2)
   (iii) Plotting the S_m against the time unit of the series
   (iv) Identifying the periods of increasing (decreasing) sub-trends in terms of the areas above (below) the reference i.e. $S_m = 0$ line

(2) Analysis of the overall trend and graphically separated sub-trends by:

   (i) Applying the statistical CRD test to verify the null hypothesis H_0 that 'there is no trend' in the full time series, and the sub-trends. For series with tied ranks, verify the H_0 by nonparametric percentile bootstrapping using Monte Carlo simulations. Trend is significant if the T_{CRD} computed using Eq. (6) falls within the $(100 - \alpha\ \%)$ confidence interval; otherwise, it is insignificant. For data with untied ranks, compare the trend statistic T_{CRD} computed using Eq. (6) with the critical value $f(n)$ from Eq. (7). If the computed $T_{CRD} < f(n)$, the linear trend is insignificant, otherwise significant.
   (ii) Computing the slope of the linear trend using the method of Theil (1950) and Sen (1968)

(3) Investigating the evolution of trend in the time series using moving window of either varying or fixed block length. Each time, the window is moved by a unit, the statistical CRD test is applied and the adjusted trend statistic T_{ADJ} (Eq. 14) is compared with the H_0 rejection/acceptance boundary limits of 1 and −1. The sub-trend for the period under consideration is significant if $T_{ADJ} > 1$ or $T_{ADJ} < -1$, otherwise insignificant.

6 Conclusion

In hydro-meteorological trend analysis, a common practice is to detect an alteration in the given variable by considering a long-term series as a whole. Whereas the long-term trend may be absent, the possible presence and significance of the hidden (short-duration) sub-trends in the series may be worth taking note of, for environmental management practices. Common trend detection methods provide rather statistical than visual exploratory aspects of the analysis. In this paper, a nonparametric CRD method was introduced to test trend in the full series and sub-trends over unknown periods of increase or decrease of the hydro-meteorological variable.

To understand its capability, the performance of the introduced method was compared with that of the well-known MK test. The trend detection power of the CRD method was shown to closely agree with that of the MK test under the various circumstances of sample sizes, variations, linear trend slopes, and serial correlation. Because the methods are nonparametric, they cannot be affected by non-normally distributed data which occur frequently in hydro-meteorology.

The introduced methods were applied to detect trend and sub-trends in the country-wide annual rainfall of the RNRCs. The co-occurrence of the changes in the rainfall with those of large-scale ocean–atmosphere interactions was analyzed in terms of trend evolutions using four climate indices or series. The long-term trends were found significant in 30 % of the RNRCs. However, the main short-duration downward (upward) sub-trends were found significant in 30 % (60 %) of the RNRCs. Generally, linkages of the trend evolutions in the rainfall of the RNRCs were found to those of the influences from the North Atlantic and Indian Oceans. Influences from the Pacific Ocean were also evident in the rainfall trend evolutions of some RNRCs. These findings are vital for planning and management of the water and agricultural practices.

For the systematic statistical methodology of the CRD considering the general case of data with or without tied ranks, the reader is referred to Onyutha (2015).

Acknowledgments The author would like to thank the three anonymous reviewers for their insightful comments and suggestions that greatly enhanced the quality of this paper. The author also wishes to acknowledge the British Atmospheric Data Centre (BADC) of the Natural Environment Research Council (NERC) for granting access to the data used in this study.

Appendix

See Fig. 10.

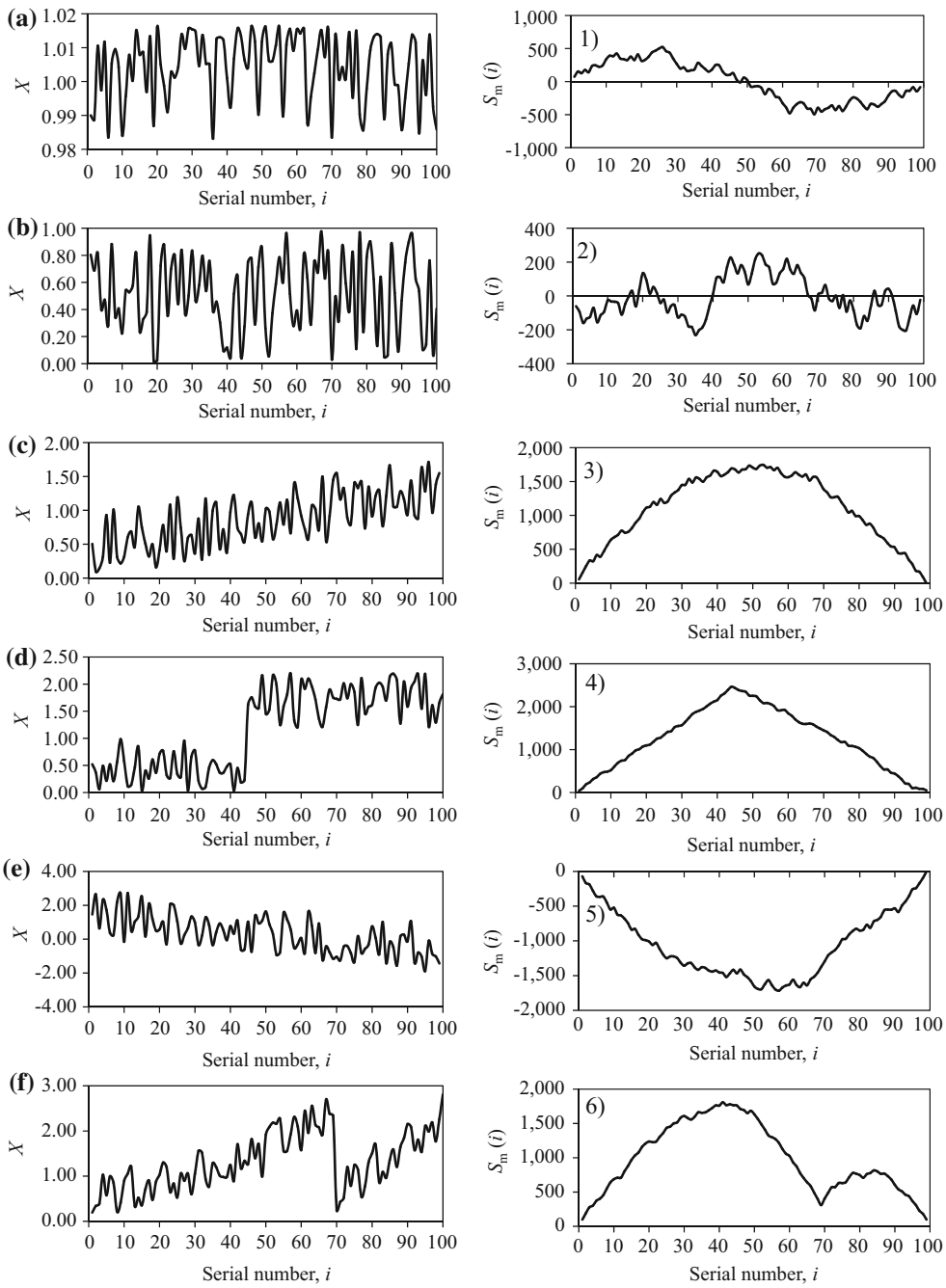

Fig. 10 CRD patterns for different cases using synthetic series, X

References

Anderson TW, Darling DA (1952) Asymptotic theory of certain goodness-of-fit criteria based on stochastic processes. Ann Math Stat 23:193–212

Buishand TA (1982) Some methods for testing the homogeneity of rainfall records. J Hydrol 58:11–27

Camberlin P (1997) Rainfall anomalies in the source region of the Nile and their connection with the Indian summer monsoon. J Clim 10:1380–1392

Davidson AC, Hinkley DV (1997) Bootstrap methods and their application. Cambridge University Press, Cambridge

Hall HS, Knight SR (1891) Higher algebra: a sequel to elementary algebra for schools, 4th edn. Macmillan & Co., New York, St. Martin's Press, London, p 596

Harris I, Jones PD, Osborn TJ, Lister DH (2014) Updated high-resolution grids of monthly climatic observations—the CRU TS3.10 Dataset. Int J Climatol 34:623–642

Hurst HE (1951) Long-term storage capacity of reservoirs. Trans Am Soc Civ Eng 116:770–799

Jury MR (2010) Ethiopian decadal climate variability. Theor Appl Climatol 101:29–40. doi:10.1007/s00704-009-0200-3

Kampata JM, Parida BP, Moalafhi DB (2008) Trend analysis of rainfall in the headstreams of the Zambezi river basin in Zambia. Phys Chem Earth 33:621–625

Kendall MG (1975) Rank correlation methods, 4th edn. Charles Griffin, London

Khaliq MN, Ouarda TBMJ, Gachon P, Sushama L, St-Hilaire A (2009) Identification of hydrologic trends in the presence of serial and cross correlations. A review of selected methods and their application to annual flow regimes of Canadian rivers. J Hydrol 368:117–130

Kizza M, Rodhe A, Xu C-Y, Ntale HK, Halldin S (2009) Temporal rainfall variability in the Lake Victoria basin in East Africa during the twentieth century. Theor Appl Climatol 98:119–135

Kolmogorov AN (1933) Grundbegriffe der Wahrscheinlichkeitsrechnung. Springer, Berlin

Kundzewicz ZW, Robson A (2000) Detecting trend and other changes in hydrological data. World climate program—water, WMO/UNESCO, WCDMP-45, WMO/TD-No. 1013. WMO, Geneva, p 157

Lavender SL, Abbs DJ (2013) Trends in Australian rainfall: contribution of tropical cyclones and closed lows. Clim Dyn 40:317–326

Mann HB (1945) Nonparametric tests against trend. Econometrica 13(3):245–259

Mantua NJ, Hare SR, Zhang Y, Wallace JM, Francis RC (1997) A Pacific interdecadal climate oscillation with impacts on salmon production. Bull Am Meteorol Soc 78:1069–1079

Modarres R, Sarhadi A (2009) Rainfall trends analysis of Iran in the last half of the twentieth century. J Geophys Res 114:D03101. doi:10.1029/2008JD010707

Moges SA, Taye MT, Willems P, Gebremichael M (2014) Exceptional pattern of extreme rainfall variability at urban centre of Addis Ababa, Ethiopia. Urban Water J 11(7):596–604

Nyeko-Ogiramoi P, Willems P, Ngirane-Katashaya G (2013) Trend and variability in observed hydrometeorological extremes in the Lake Victoria basin. J Hydrol 489:56–73

Onyutha C (2014) Variability of seasonal and annual rainfall in the River Nile riparian countries and possible linkages to the ocean-atmosphere interactions. Hydrol Res (Under review after revision)

Onyutha C, Willems P (2014) Spatial and temporal variability of rainfall in the Nile basin. Hydrol Earth Syst Sci Discuss 11:11945–11986

Onyutha C (2015) Analyses of hydrometeorological trend/sub-trends using nonparametric cumulative rank difference method. Stoch Environ Res Risk Assess. (Under review)

Paruolo P, Murphy B, Janssens-Maenhout G (2014) Do emissions and income have a common trend? A country-specific, time-series, global analysis, 1970–2008. Stoch Environ Res Risk Assess. doi:10.1007/s00477-014-0929-9

Ropelewski CF, Jones PD (1987) An extension of the Tahiti-Darwin southern oscillation index. Monday Weather Rev 115: 2161–2165

Sen PK (1968) Estimates of the regression coefficient based on Kendall's tau. J Am Stat Assoc 63:1379–1389

Şen Z (2012) An innovative trend analysis methodology. J Hydrol Eng 17:1042–1046

Şen Z (2014) Trend identification simulation and application. J Hydrol Eng 19:635–642

Smirnov NV (1936) Sur la distribution de w2 (criterium de M. R. von Mises). C R Acad Sci 202:449–452

Sneyers R (1990) On the statistical analysis of series of observations. Technical note 143, WMO, Geneva, p 192

Sonali P, Kumar ND (2013) Review of trend detection methods and their application to detect temperature changes in India. J Hydrol 476:212–227

Stephens MA (1986) Tests based on EDF statistics. In: D'Agostino RB, Stephens MA (eds) Goodness-of-fit techniques. Marcel Dekker, New York. ISBN 0-8247-7487-6

Tao H, Fraedrich K, Menz C, Zhai J (2014) Trends in extreme temperature indices in the Poyang Lake Basin, China. Stoch Environ Res Risk Assess 28:1543–1553. doi:10.1007/s00477-014-0863-x

Taye MT, Willems P (2012) Temporal variability of hydroclimatic extremes in the Blue Nile basin. Water Resour Res 48:W03513. doi:10.1029/2011WR011466

Theil H (1950) A rank-invariant method of linear and polynomial regression analysis. Nederl Akad Wetench Ser A 53:386–392

Tierney JE, Smerdon JE, Anchukaitis KJ, Seager R (2013) Multidecadal variability in East African hydroclimate controlled by the Indian Ocean. Nature 493:389–392

van Oldenborgh GJ, te Raa LA, Dijkstra HA, Philip SY (2009) Frequency-or amplitude-dependent effects of the Atlantic meridional overturning on the tropical Pacific Ocean. Ocean Sci 5:293–301. doi:10.5194/os-5-293-2009

Vogel RM (1986) The probability plot correlation coefficient test for the normal, lognormal, and Gumbel distributional hypotheses. Water Resour Res 22:587–590

Yue S, Pilon P, Phinney B, Cavadias G (2002a) The influence of autocorrelation on the ability to detect trend in hydrological series. Hydrol Process 16:1807–1829

Yue S, Pilon P, Cavadias G (2002b) Power of the Mann–Kendall and Spearman's rho tests for detecting monotonic trends in hydrological series. J Hydrol 259:254–271